Efficient CFD Modeling of Bulk Condensation, Fog Transport and Re-Evaporation for Application to Containment Scale

Allen George[a,b,*], Stephan Kelm[a], Xu Cheng[b], Hans-Josef Allelein[a]

[a] *Institute of Energy and Climate Research, Forschungszentrum Jülich GmbH, Jülich, Germany*
[b] *Institute for Applied Thermofluidics (IATF), Karlsruhe Institute of Technology, Karlsruhe, Germany*

Abstract

Formation of fog due to bulk condensation during a Beyond Design Basis Accident (BDBA) in a water-cooled nuclear reactor is of high safety relevance with regard to the flammability of the containment atmosphere and its interaction with several other safety relevant phenomena such as aerosol transport. Bulk condensation of steam in the presence of non-condensable gases is modelled using 'return to saturation in constant timescale' method in single-phase system as mass sink. The fog droplets formed as a result of condensation is transported as passive scalar in an Eulerian frame by considering the effects of convection by the gas mixture, turbulent and Brownian diffusion and droplet drift due to gravitation, drag and inertial forces. The model formulation is based on the assumption that fog volume fraction is fairly low ($< 1\%$) so that droplet-droplet interactions and the effect droplets on the gas flow are negligible. The present work considers only spherical fog droplets of fixed diameter and evolution of droplet by coalescence and breakup is neglected. The effect of different droplet sizes is investigated in the validation cases to understand its consequence on the results. It is also assumed that the fog droplets are always in thermal equilibrium with the surrounding gas mixture. The re-evaporation of the transported fog droplets in regions where gas temperature is higher than saturation temperature is also incorporated into the solver. The model was numerically implemented to the containmentFOAM CFD package based on OpenFOAM. The verification of the phase change(condensation & evaporation) model by simulating the mixing of a cold and hot air-steam-fog mixture gave good agreement with Mollier diagram theory in terms of both final mixture temperature and quantity of steam and fog. The droplets drift transport model was validated by aerosol flow through a bent pipe investigating the effect of droplet Stokes number on deposition efficiency. The performance of the bulk condensation model was further validated and assessed by including the interaction with other rele-

*Correspondence: a.george@fz-juelich.de; Tel.: +49 2461 85265

vant containment phenomena (e.g., wall condensation, multispecies transport) on SETCOM experimental facility (Forschungszentrum Jülich, Germany) and a technical scale THAI experiment (Becker Technologies, Germany). The results indicated that the inclusion of bulk condensation model improved the predictive capabilities of *containmentFOAM*, i.e., the consistency of simulation and measurements for these experiments.

Keywords: Bulk condensation, reactor containment, fog transport, droplet drift, passive scalar, containmentFOAM

Nomenclature

α_{fog}	Fog volume fraction (m^3/m^3)
Δt	Time step size for simulation (s)
$\dot{m}$	Mass flow rate ($kg\,s^{-1}$)
η	Deposition efficiency
λ	Laminar thermal conductivity of the gas mixture ($W\,m^{-1}\,K^{-1}$)
μ	Dynamic viscosity of the gas mixture ($kg\,m^{-1}\,s^{-1}$)
ν	Kinematic viscosity of the gas mixture ($m^2\,s^{-1}$)
ν_t	Turbulent kinematic viscosity of the gas mixture ($m^2\,s^{-1}$)
ω	Turbulent eddy frequency
ρ	Gas mixture density ($kg\,m^{-3}$)
ρ_{fog}	Fog density or fog mass per unit volume ($kg\,m^{-3}$)
ρ_{water}	Fog material(water) density ($kg\,m^{-3}$)
τ	Viscous stress tensor $kg\,m^{-1}\,s^{-2}$)
τ_{fog}	Fog droplet relaxation time (s)
$\vec{S}_U$	Volumetric momentum source term ($kg\,m^{-2}\,s^{-2}$)
$\vec{U}$	Gas mixture velocity vector ($m\,s^{-1}$)
$\vec{u}_d$	Fog droplet drift velocity vector ($m\,s^{-1}$)
$\vec{u}_p$	Fog droplet total velocity vector ($m\,s^{-1}$)
C_p	Specific heat capacity of the gas mixture ($J\,kg^{-1}\,K^{-1}$)
C_c	Cunningham correction factor
C_{p,H_2O}	Specific heat capacity of steam species in the gas mixture ($J\,kg^{-1}\,K^{-1}$)
D_B	Brownian diffusivity of the fog droplets ($m^2\,s^{-1}$)
D_j	Molecular diffusivity of j-th gas species in the mixture ($m^2\,s^{-1}$)
D_t	Turbulent diffusivity ($m^2\,s^{-1}$)
d_{fog}	Fog droplet diameter (m)

g	Gravitational acceleration ($m\,s^{-2}$)
h	Static enthalpy of the gas mixture ($J\,kg^{-1}$)
h_{fg}	Latent heat of vaporization ($J\,kg^{-1}$)
h_j	Specific enthalpy of j-th gas species ($J\,kg^{-1}$)
h_{tot}	Total enthalpy of the gas mixture ($J\,kg^{-1}$)
k	Turbulent kinetic energy ($J\,kg^{-1}$)
k_B	Boltzmann constant ($J\,K^{-1}$)
p	Pressure (Pa)
p_{H_2O}	Partial pressure of steam species in the gas mixture (Pa)
Pr_t	Turbulent Prandtl number
Q	Energy source term for the gas mixture during phase change($W\,m^{-3}$)
Q_v	Effective energy source term for the gas mixture during phase change($W\,m^{-3}$)
Q_{cond}	Energy source term for the gas mixture during condensation($W\,m^{-3}$)
Q_{evap}	Energy source term for the gas mixture during evaporation($W\,m^{-3}$)
R	Radius of the bent pipe (m)
S_{H_2O}	Volumetric mass source term for the steam gas species($kg\,m^{-3}\,s^{-1}$)
S_h	Volumetric energy source term for the gas mixture($W\,m^{-3}$)
S_j	Volumetric mass source term for the j-th gas species($kg\,m^{-3}\,s^{-1}$)
S_m	Volumetric mass source term for the gas mixture($kg\,m^{-3}\,s^{-1}$)
Sc_t	Turbulent Schmidt number
St	Stokes number
T	Temperature of the gas mixture (K)
T_{sat}	Saturation temperature of the gas mixture (K)
x	Water vapor(steam) content
Y_j	Mass fraction of j-th gas species
Y_{H_2O}	Mass fraction of steam species in the gas mixture

1. Introduction

During a Beyond Design Basis Accident (BDBA) in a water-cooled nuclear reactor, large amounts of steam and combustible gases (H2/CO) are released

into its containment. Condensation of steam into water can occur on walls as well in the bulk in the form of droplets depending on the local state of the gas mixture and saturation conditions. Bulk condensation of steam in the presence of non-condensable gases (NCGs) influences the local mixture composition, transient pressure and temperature, hydrogen flammability and gas radiation (scattering by fog droplets) and must be considered in containment thermal hydraulics.

In the event of a postulated accident scenario like loss-of-coolant accident (LOCA), large amounts of steam are released into the containment atmosphere. The partial pressure and consequently, the saturation temperature of steam gradually increases and when the mixture temperature is lower than the steam saturation temperature, the excess steam get condensed in the form of droplets. Previous studies by Vyskocil et al. (2014) in a single-phase framework considered fog condensed as a mass sink and removed it from the control system. The transport of the fog droplets and its re-evaporation is neglected in this model. Zhang and Laurien (2014) implemented a two-fluid model where fog is treated as separate phase from the steam-NCGs mixture. However, this model involves solving two sets of conservation equations and modelling of transfer terms which is computationally expensive for large scale containment simulations. One drawback of this model formulated based on interfacial area density is that condensation can occur only on droplet surfaces. Hence, an initial amount of fog is needed to be present in the entire computational domain at the start of the simulation for condensation to occur. Babić et al. (2009) used a combination of Lagrangian approach for fog droplet tracking and general purpose CFD code CFX for the continuous gas phase for simulating containment sprays. The fog–gas interaction was modelled with sinks of momentum, heat and mass, calculated with the Lagrangian droplet-tracking code. The model was able to predict the experimental data reasonably well and reproduce the non-homogeneous structure of the gas atmosphere in TOSQAN vessel. Ding et al. (2017) investigated the condensation and evaporation of droplets inside containment using GASFLOW code and compared homogeneous and Lagrangian approaches. The homogeneous(passive scalar) approach considered the fog as a component of the continuous gas phase and assumed that the droplets share the same velocity field with the gas. In the Lagrangian approach, the transport and evolution(heat and mass transfer) of fog droplets is modelled using Lagrangian particle tracking method. They found that the Lagrangian tracking approach gave much better agreements for pressure, temperature and gas volume fraction with the experimental data. However, the droplet deviation from gas flow path due to drift was not considered in the homogeneous approach and this method can capture some features of the Lagrangian approach with relatively less computational power.

The aim of the present work is to develop a computationally efficient, simplified bulk condensation model considering the formation, transport, evaporation and effects of fog inside a nuclear reactor containment. It involves transport of the fog in an Eulerian framework as a passive scalar such that it does not directly influence the flow field of the gas mixture. The fog evolution mechanism

considers the condensation and evaporation in the form of constant diameter droplets. The fog droplets are then transported by the effects of convection (velocity field of the gas mixture), turbulent and Brownian diffusion and also by drift (drag, gravitational and inertial forces). The model is implemented to the *containmentFOAM* (Kelm et al., 2021) CFD package based on OpenFOAM to understand the combined effects of several phenomena such as multi-species transport, turbulence, wall condensation, gas radiation and aerosol transport. The performance of the condensation and evaporation model is verified by Mollier diagram theory (Mollier, 1929) and the fog drift transport model is validated against the droplet(aerosol) deposition experiments (Pui et al., 1987) and simulations (Pilou et al., 2011; Frederix et al., 2017) inside a bent pipe geometry. The improvement in predictive capabilities by the model is demonstrated by SETCOM (Kelm et al., 2019) and THAI TH2 (T. Kanzleiter, 2002) experiment simulations.

2. Modelling Approach

Containment thermal hydraulics is modelled as single phase phenomenon where the conservation equations are solved for the gas mixture phase using an unsteady Reynolds Averaged Navier Stokes (U-RANS) approach. The effect of bulk condensation is included as source/sink terms in these equations. However, the mass of steam removed from the mixture system by condensation in the form of fog is not neglected. It is transported as a passive scalar in an Eulerian framework in the computational domain and is also allowed to re-evaporate. The mathematical formulation is derived from the original containmentFOAM governing equations (Kelm et al.) by adding volumetric source/sink terms due to condensation/evaporation.

2.1. Governing equations

Mass continuity equation:

$$\frac{\partial \rho}{\partial t} + \nabla \cdot (\ \rho \vec{U}) \ = S_m \tag{1}$$

Momentum transport equation:

$$\frac{\partial \rho \vec{U}}{\partial t} + \nabla \cdot \left(\rho \vec{U} \otimes \vec{U} \right) = -\nabla p + \nabla \cdot \tau + \rho \vec{g} + \vec{S}_u \tag{2}$$

with the full buoyancy model $\rho \vec{g}$ and the shear stress tensor:

$$\tau = \rho \left(\nu + \nu_t \right) \left[\nabla \vec{U} + \left(\nabla \vec{U} \right)^T - \frac{2}{3} \delta \nabla \cdot \vec{U} \right] \tag{3}$$

Energy transport equation:

$$\frac{\partial \rho h_{tot}}{\partial t} + \nabla \cdot \left(\rho \vec{U} h_{tot}\right) = \rho \vec{U} \cdot \vec{g} + \frac{\partial p}{\partial t} + \nabla \cdot \left[\left(\lambda + \frac{C_p \nu_t}{Pr_t}\right) \nabla T\right] + \sum_j \nabla \cdot \left[\rho h_j \left(D_j + D_t\right) \nabla Y_j\right] + S_h \tag{4}$$

where the total enthalpy $h_{tot} = h + \frac{1}{2}|\vec{U}|^2$.

Species transport equation:

$$\frac{\partial \rho Y_j}{\partial t} + \nabla \cdot \left(\ \rho \vec{U} Y_j\right) \ = \nabla \cdot \left[\rho \left(D_j + D_t\right) \nabla Y_j\right] + S_j \tag{5}$$

2.2. Bulk condensation modelling

The bulk condensation process is modelled using the "*return to saturation in a constant timescale*" method by Vyskocil et al. (2014). This method in principle works by making the mixture saturated locally at all times by either condensing the excess steam or by evaporating the excess fog droplets. The energy needed for heating the local mixture to saturation temperature is released during condensation to fog in numerical time step Δt. Similarly, during the evaporation of the fog, an equivalent amount of energy required for cooling the local mixture to saturation temperature is absorbed. The fog droplets are assumed to be always in local thermal equilibrium with the surrounding gas mixture and hence will have same temperature of local gas mixture.

$$Q = \rho C_p \frac{T_{sat}(p_{H_2O}) - T}{\Delta t} \tag{6}$$

If $T < T_{sat}(p_{H_2O})$ in a mesh element, condensation occurs ($Q > 0$) and temperature in the element increases to saturation temperature. Similarly, if $T > T_{sat}(p_{H_2O})$, evaporation occurs ($Q < 0$) and temperature in the element decreases to saturation temperature. However, the energy Q must be limited by the mass of steam or fog available within an element to prevent any mass and energy conservation issues.

$$Q_{cond} = \rho Y_{H_2O} \frac{h_{fg}}{\Delta t} \tag{7}$$

$$Q_{evap} = -\rho_{fog} \frac{h_{fg}}{\Delta t} \tag{8}$$

Finally, the Eqns. 6, 7 and 8 are combined to formulate the volumetric enthalpy transfer term during phase change process.

$$\begin{cases} if \quad Q > 0 \quad (condensation), \quad Q_v = min(Q, Q_{cond}) \\ if \quad Q < 0 \quad (evaporation), \quad Q_v = max(Q, Q_{evap}) \end{cases} \tag{9}$$

The volumetric source/sink terms in the Eqns. 1 - 5 are then computed from the enthalpy transfer term Q_v as described below.

$$\text{Mass transfer term:} \quad S_m = -\frac{Q_v}{h_{fg}} \tag{10}$$

$$\text{Momentum transfer term:} \quad \vec{S}_u = S_m \vec{U} \tag{11}$$

$$\text{Energy transfer term:} \quad S_h = Q_v + S_m C_{p,H_2O} T \tag{12}$$

$$\text{Species mass transfer term:} \quad S_{H_2O} = S_m \tag{13}$$

2.3. Fog transport modelling

The fog mass generated by bulk condensation will be in the form of droplets and gets suspended in the carrier phase (gas mixture). However, due to their different physical properties from the gas mixture, the droplets tends to deviate from the carrier gas velocity field. This motion known as drift is induced by the combined effects of inertia, gravity and drag. Also, the bombardment of the gas molecules on the droplets may cause random motion called Brownian motion of the droplets. This will lead to the diffusion of droplets and is significant when droplet sizes are sufficiently small. In a turbulent flow, the droplet transport due to turbulent diffusion also has to be included. Considering all these effects, the fog transport equation is developed:

$$\frac{\partial \rho_{fog}}{\partial t} + \nabla \cdot \left[\rho_{fog} \left(\vec{U} + \vec{u}_d \right) \right] = \nabla \cdot \left[\left(D_B + D_t \right) \nabla \rho_{fog} \right] - S_m \tag{14}$$

The fog transport equation (Eqn.14) is formulated by neglecting the droplet-droplet interactions and effect of droplet on the gas flow which is valid for fog volume fractions ($\alpha_{fog} = \rho_{fog}/\rho_{water}$) below 1 %. The droplet drift velocity and Brownian diffusivity values largely depends on the droplet diameter. In the present work, the droplet diameter is fixed for each simulation and evolution of fog size by coalescence and breakup is neglected. The droplet diameter values used for each validation case is decided based on the values available from experiments and a droplet diameter dependency study also performed for relevant cases. The droplet drift velocity can be computed using force balance equation for droplet as described in Manninen et al. (1996) and Frederix et al. (2017). The Partial Differential Equation (PDE) form of this equation is given by:

$$\frac{\partial \vec{u}_p}{\partial t} + \left(\vec{u}_p \cdot \nabla \right) \vec{u}_p = -\frac{1}{\tau_{fog}} \left(\vec{u}_p - \vec{U} \right) + \left(\frac{\rho_{water} - \rho}{\rho_{water}} \right) \vec{g} \tag{15}$$

where $\vec{u}_p = \vec{u}_d + \vec{U}$ and $\tau_{fog} = \frac{\rho_{water} d_{fog}^2}{18\mu}$

The Eqn.15 is known as Stokes model and can be solved numerically like other conservation equations. To reduce the computational effort in solving this equation, Manninen et al. (1996) approximated the PDE based on local equilibrium assumption that the acceleration of the droplet is equal to the acceleration of the gas mixture (Eqn. 16).

$$\frac{\partial \vec{u}_p}{\partial t} + (\vec{u}_p \cdot \nabla)\, \vec{u}_p \approx \frac{\partial \vec{U}}{\partial t} \tag{16}$$

The Stokes as well as Manninen drift velocity models are considered in the present work and their performance is compared.

The droplet size-dependant Brownian diffusivity is calculated using Stokes-Einstein equation (Hinds, 1999; Frederix et al., 2017) which provides a model for diffusivity of a spherical body like droplets in this work.

$$D_B = \frac{k_B C_c T}{3\pi\mu d_{fog}} \tag{17}$$

2.4. Turbulence Modelling

Turbulence in the gas mixture phase is modelled by standard $k-\omega$ SST model of Menter and Esch (2001) which solves transport equations for turbulent kinetic energy k and eddy frequency ω. The source terms for the turbulent transport equations are $S_k = S_m k$ and $S_\omega = S_m \omega$ which are treated implicitly for condensation and explicitly for evaporation. In the simulations presented in this paper, the gas mixture is considered as compressible and fog material (water) is modelled with constant density ($\rho_{water} = 1000 kg/m^3$). The molecular diffusivity of each species in the gas mixture is calculated using effective binary diffusivity approximation and turbulent diffusivity is defined as $D_t = \nu_t / Sc_t$. The mass diffusion due to temperature gradient (Soret effect) is neglected in this study. Also, the turbulent Schmidt number (Sc_t) is chosen to have same value of turbulent Prandtl number (Pr_t), i.e., $Pr_t = Sc_t = 0.85$ in all simulations. The thermo-physical properties of the mixture like specific heat capacity (C_p), thermal conductivity (λ) and dynamic viscosity (μ) are evaluated using the Wilke's relation (Wilke, 1950).

3. Results and Discussions

The analytical and experimental works investigated to verify and validate each model aspect is shown in Table. 1. The bulk condensation and evaporation models are initially verified using Mollier diagram (Siemens, 2007) by using a mixing nozzle as in Zhang and Laurien (2014) to simulate the conditions similar to that in the diagram. Following this, the fog transport model is validated based on deposition of droplets on the walls of bent pipe due to drift velocity which is predominantly due to the inertia of these droplets. The drift of droplet due to gravity is validated by using the analytical equation of a droplet(or

particle) falling under gravity in stationary atmosphere however, this is not explicitly discussed in this paper. Then we have the SETCOM experiment which is primarily designed to investigate wall condensation, yet, bulk condensation also occur near the walls which has notable effects on the results. Re-evaporation of the condensed fog is also included in the simulation, although its effects are a marginal in the SETCOM case. Finally, the combined effect of all the models is validated against the ThAI TH2 experiment. In all these simulations, the maximum fog volume fraction is below 1% and the thermal Stokes number is very small so that the simulations adhere to the model assumptions. The effect of droplet diameter on the results is also addressed for each validation case.

Table 1: Experiments for verification and validation of models

Experiments	Bulk condensation model		Fog transport model		
	Condensation	Evaporation	Inertia	Gravity	Diffusion
Mollier Diagram	✓	✓			
Bent pipe deposition			✓		
SETCOM experiment	✓	✓			✓
THAI TH2 experiment	✓	✓	✓	✓	✓

In the validation experiments (SETCOM and THAI) considered in the work, bulk condensation is an additional phenomenon happening along with wall condensation, and we examine the combined effect of both phenomena. In containmentFOAM, wall condensation is modelled as an outflux on the condensing wall in the form of boundary condition. The wall condensation model implementation and its validation with SETCOM experiment is discussed in Kumar et al. (2021). In this simplified single-phase approach, the mass of water formed due to condensation on walls is removed from the computational domain and disregarded. The transport of the fog as a passive scalar in a single-phase framework is valid only at lower volume fraction of fog ($< 1\%$) and hence, cannot model high deposition and accumulation of fog on walls resulting in the formation of free water surfaces. So, for simulations involving large deposition of fog on wall, a zero gradient boundary condition is used on the walls to remove the excess fog from the system to prevent unphysical fog density values near walls. The coverage of walls with films, rivulet or droplets and also the accumulation of the condensate near walls and its effects is beyond the scope of this work and require two-phase approach which will of interest in the future.

3.1. Mollier diagram verification

The Mollier diagram (Mollier, 1929), also known as *ix* diagram is a graphical representation of thermodynamic properties of steam. It is based on the relationship between the heat content(enthalpy) and water vapour content of the air. The heat content is difficult to measure directly, so the diagram is also included with temperature and relative humidity which are relatively easier to measure. The bulk condensation model is verified using the Mollier diagram (Siemens, 2007) by considering the mixing process of hot and cold air-steam mixture such

that the mixing point is below saturation line. Similarly, the evaporation model is verified by mixing a hot air-steam mixture with a cold air-steam-fog mixture with an initial amount of fog present in the cold mixture. The initial conditions of mixtures before mixing for both condensation and evaporation cases are shown in Table 2.

Consider two air flows with mass flow rates $\dot{m}_1$ and $\dot{m}_2$ having different states Z_1 and Z_2 are mixed. This will result in a third state Z_m whose properties can be determined using the Mollier diagram. The mixing point will divide the line joining the Z_1 and Z_2 into two sections such that mixing point is closer to the air state of the larger of the two mixed quantities.

Table 2: Properties of the two states Z_1 and Z_2 for condensation and evaporation processes from Mollier diagram

	Condensation		Evaporation	
	State Z_1	State Z_2	State Z_1	State Z_2
Temperature $[^oC]$	26	-10	26	9.5
Vapor content $[g/kg]$	17	1.1	17	7.4
Fog content $[g/kg]$	0	0	0	1.1
Relative humidity [%]	80	70	80	100
Density $[kg/m^3]$	1.18	1.34	1.18	1.26

The state of the mixing point M can be computed by (e.g. , vapour content)

$$x_M = \frac{x_1\dot{m}_1 + x_2\dot{m}_2}{\dot{m}_1 + \dot{m}_2}[g/kg] \tag{18}$$

where vapor content, $x = m_{steam}/m_{air}$
Similarly, the specific enthalpy at the mixing point is calculated by

$$h_M = \frac{h_1\dot{m}_1 + h_2\dot{m}_2}{\dot{m}_1 + \dot{m}_2}[kJ/kg] \tag{19}$$

The h_M and T_M will give the location of the mixing point on the Mollier diagram and other state properties can be interpreted from the diagram.

When the mixing point is below the saturation line (100 % relative humidity), the air is over-saturated at that point, i.e., it contains an excess amount of water relative to its temperature. If the temperature of the air is left unchanged, the surplus vapour is removed by condensation and is held in the air in the form of fine droplets as fog or mist. Similarly, when excess fog is present in the air relative to its saturation temperature, the surplus is removed by evaporation of fog to vapor. The air state moves in the direction of mist isotherms and reaches the saturation point. The final mixture state properties like temperature and vapour content are measured at the saturation point and the difference in the vapour content between states gives the amount of fog formed.

Following the work by Zhang and Laurien (2014), the mixing process is

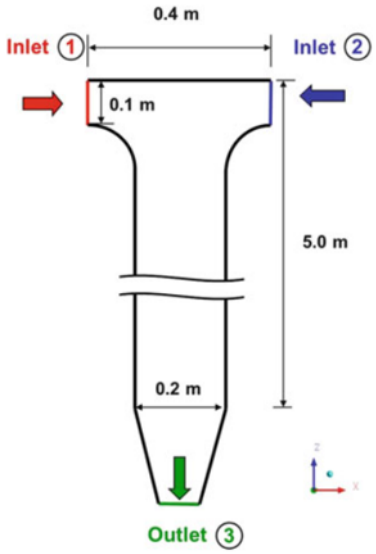

Figure 1: Mixing nozzle Geometry (Zhang and Laurien, 2014)

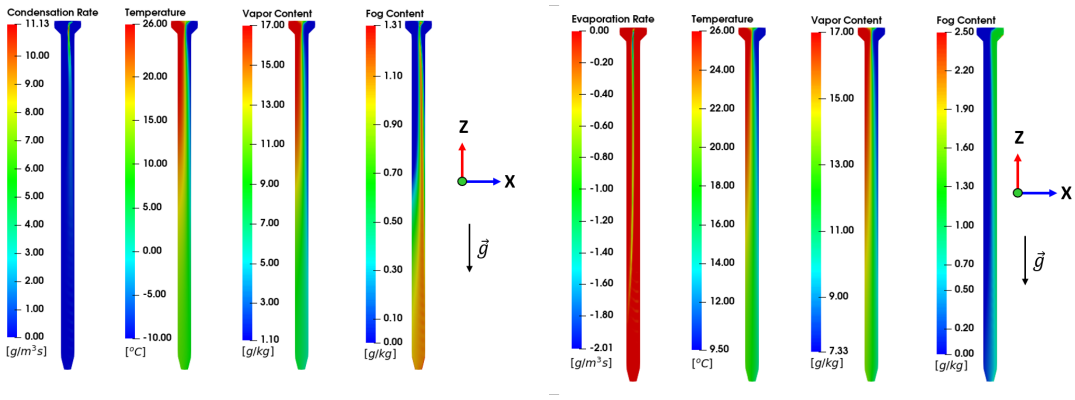

(a) (b)

Figure 2: Mass transfer rate, temperature, vapor content and fog content distributions in the mixing nozzle after steady state for condensation(a) and evaporation(b) cases

simulated in containmentFOAM on a two-dimensional mixing nozzle with two inlets until steady state is achieved. The geometry of the nozzle is shown in Fig. 1 and the boundary conditions are taken from Table 2. The nozzle is made long enough (5 m) to ensure full mixing of the wet air flows. Computations have been performed on two meshes, a coarse mesh with 2700 elements and a fine mesh with 10800 elements. The deviation in results between coarse and fine mesh were less than 0.1 % and the fine mesh results are presented here. The simulation results (Fig. 2) indicate that condensation (or evaporation) occurs primarily

in the upper portion and the mixture is well mixed before reaching the outlet. The condensation (or evaporation) rate is almost zero towards the end of the channel, and the condensed fog is transported by the flow through the outlet. For both condensation and evaporation cases, it is the thermodynamic balance between both processes that maintains the mixture at saturation state. i.e., for condensation validation case, some evaporation also occurs which is relatively small and vice-versa. However, to focus on major processes in the respective cases, the mass transfer rate contours in Fig. 2 displays only dominant rates. The mixture properties at the outlet are compared with Mollier diagram (Table 3) and the temperature, vapor and fog content are accurate within 6 %, thus confirming good agreement of the model to the theory. The droplet diameter chosen for this simulation is 25 μm however, the results are independent of the diameter as drift and Brownian diffusion were neglected in this case. Also, the maximum fog volume fraction was observed to be $<<$ 1% which is well within the modelling assumptions.

Table 3: Comparison between Mollier diagram theory and simulation result

	Condensation			Evaporation		
	Mollier	Simulation	Error(%)	Mollier	Simulation	Error(%)
Gas Temperature $[^oC]$	9.5	9.7	2.1	17	17.27	1.57
Vapor content $[g/kg]$	7.4	7.35	0.6	12.2	12.19	0.01
Fog content $[g/kg]$	1.1	1.13	2.7	0.4	0.42	6.01

3.2. The bent pipe deposition

The drift transport model is validated with the inertial deposition of aerosol (droplet) experiment in a bent pipe. Cheng and Wang (1981) analytically investigated the depostion data whereas Pui et al. (1987) examined it experimentally. Pilou et al. (2011) numerically modelled the aerosol flow and deposition in an Eulerian-Eulerian framework with one-way coupling similar to the method used in the present work. This simulation follows the work done by Frederix et al. (2017), and the bent pipe geometry and mesh used for the simulation are shown in Fig. 3.

The deposition efficiency of an airborne droplet as a function of the Stokes number is simulated for model validation. The Stokes number (St) is defined as the ratio of the droplet inertial timescale over the flow convective timescale and is given by:

$$St = \frac{\rho_p d_p^2 C_c U}{18 \mu R} \tag{20}$$

.

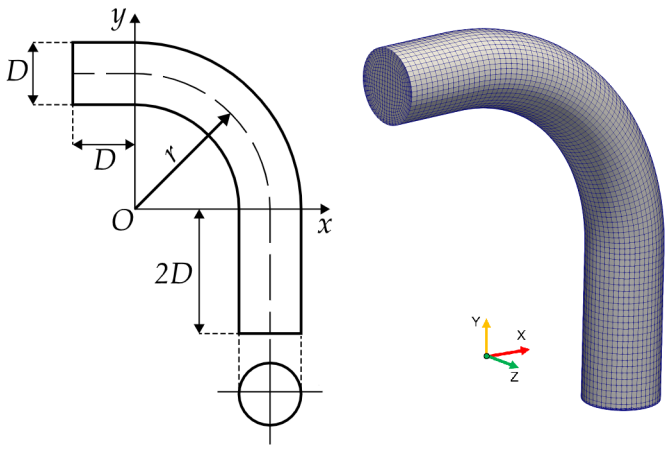

Figure 3: Left: Geometry of the bent pipe (Frederix et al., 2017). Right: 3D computational mesh of the bent pipe

The deposition efficiency (η) is defined as ratio of droplet mass depositing on the wall to the inlet droplet flow mass given by:

$$\eta = \frac{\dot{m}_{deposit}}{\dot{m}_{inlet}} \tag{21}$$

where $\dot{m}_{deposit}$ is the droplet mass deposition rate and $\dot{m}_{inlet}$ is the droplet mass inflow rate.

The deposition efficiency simulations were performed for 11 different droplet diameters between 4 μm and 15 μm at flow Reynolds number = 1000 similar to the experiment (Pui et al., 1987). The simulation parameters used are specified in Table. 4.

Table 4: Fluid, droplet properties and pipe parameters used in simulations

Fluid temperature T	273 K
Fluid density ρ	1.18 kg/m^3
Fluid dynamic viscosity μ	1.85×10^{-5}
Droplet diameters d_p	4−15 μm
Droplet material density ρ_p	895 kg/m^3
Pipe diameter D	$3.95 \times 10^{-3} m$
Pipe bend radius of curvature r	$22.515 \times 10^{-3} m$
Fluid mean inlet velocity U	$3.86 m/s$

The flow while passing through the bend gets accelerated due to change in direction and the large droplets because of their high inertia deviate from the gas flow path and gets deposited on the walls. However, small droplets with low

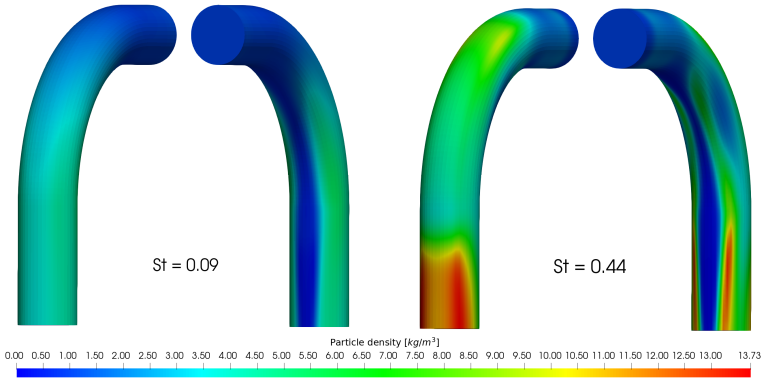

Figure 4: Droplet concentration on the wall at two different Stokes numbers

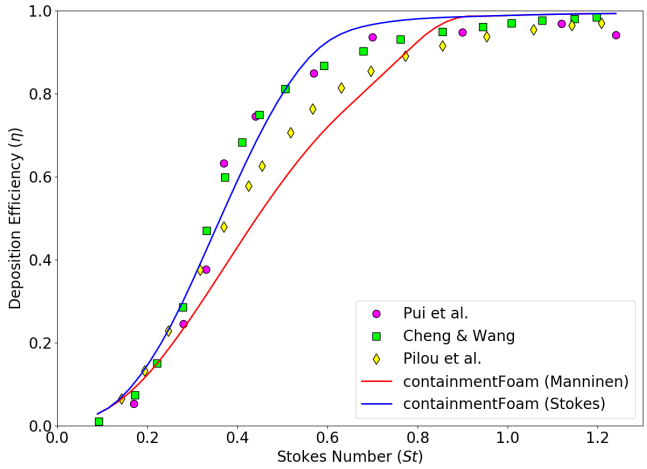

Figure 5: Inertial deposition efficiency as a function of Stokes number - experiment vs simulations

inertia can closely follow the streamlines and reach the outlet. This is demonstrated by the droplet deposition concentration contour in Fig. 4. For low Stokes number, the outer bend is almost uniformly covered with a layer of droplets. There is vertical strip free of droplets in the inner bend. Also, majority of the droplets are deposited after the mid-bend. However, at high Stokes numbers, the droplet deposition is more at the start and end of the bend. This is due to the higher inertia of the droplet which make it easier for them to deviate from the streamlines even at locations close to the start of bend. At locations near the end of bend, there are counter-rotating vortices which aids the high inertia droplets to drift away and get deposited. The prediction of deposition efficiency

using Stokes and Manninen drift velocity models is compared with the already available literature (Fig. 5). The Stokes number of the droplets were varied by using 11 different diameters in the range 4-15 μm while keeping other simulation parameters fixed. The computed deposition efficiency by Stokes drift model is in closer agreement with the analytical(Cheng and Wang, 1981) and experimental(Pui et al., 1987) results compared to the numerical model by Pilou et al. (2011) for all range of Stokes numbers. The Manninen model prediction is good at low and high Stokes numbers but, underestimates the deposition efficiency at medium Stokes numbers. The Stokes drift model predicts the deposition efficiency with reasonable accuracy at all range of Stokes number and will be used for further simulations. These results also indicate that the droplet diameter is an important parameter in high inertia flows. As the droplet diameter is fixed for a simulation in the current work, the effects of different diameters on the results are investigated in subsequent simulations.

3.3. SETCOM experiment validation

The SETCOM (Separate Effects Tests for Condensation Modelling) facility at Forschungszentrum Jülich is operated to provide validation data for condensation modelling. The test section consists of 6 m long rectangular flow channel of cross-section 0.44 m $\times$ 0.44 m with three adiabatic walls and a cooled wall over which condensation occurs. The experiment facility can also be inclined between a horizontal to vertical position allowing measurements in forced as well as mixed convection regimes. The geometry and facility is explained in detail in Kelm et al. (2019). The SETCOM experiment was previously used to validate wall condensation model (Kumar et al., 2021) in containmentFOAM where a single-phase mass sink approach is used on walls to remove the wall condensate and fog formation in regions near the condensing wall was not considered in the model. The present work focuses on including the effect of fog also into the mathematical model and how it affects the prediction capability. It is important to note that the water film, rivulets or droplets formed on wall due to wall condensation is removed from the computational domain whereas fog mass is transferred to a passive scalar variable, transported and available for re-evaporation.

The addition of bulk condensation model into containmentFOAM has given the possibility of simulating the effect of fog in steam-NCG gas mixture flows close to the saturation region. From the SETCOM database consisting of 81 experiments from mild to severe condensation rate, an experiment with vertical steam-air mixture flow was randomly chosen to investigate the fog effect ($U_{in} \approx 4.2$ m/s, $T_{in} \approx 80$ ^{o}C, $X_{H2O,in} \approx 30$ vol.%, $T_{coolant} \approx 10$ ^{o}C). For the wall temperature, a heat flux (including condensation wall heat flux) boundary condition was used to compute temperature from heat transfer coefficient and coolant temperature($T_{coolant}$). The wall condensation computations by Kumar et al. (2021) on a fine mesh ($y^+ \approx 1$) and a coarse mesh ($y^+ \approx 75$) found that the coarse mesh predictions deviated from experimental values in the developing region of flow ($x < 1m$) whereas the fine mesh predictions were reasonably good in all regions. Hence, the fine mesh with $y^+ \approx 1$ is selected for bulk condensation

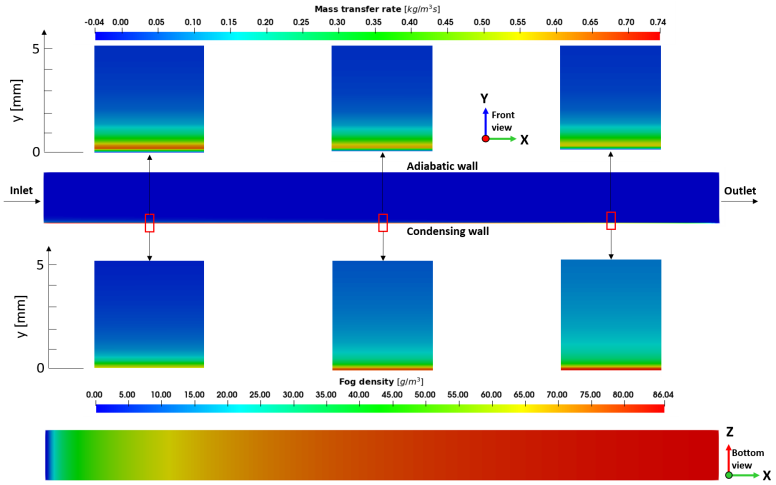

Figure 6: Fog formation rate (top) and fog density distribution (bottom) at different locations near the cooled wall in SETCOM 2D simulation

simulation in the present work. The simulation results after attaining steady state (Fig. 6) indicates the formation of fog droplets at regions very close to the cool wall ($x \approx 1 - 5mm$). The maximum bulk condensation occurs in cells next to the near wall cells, because bulk condensation is deactivated in cells where wall condensation occurs to prevent repetitive removal of same steam mass by both models. The bulk condensation is highest near the inlet region ($x = 0 - 1m$) and gradual decreases downstream as the mixture becomes more and more saturated. The droplets get transported by the effects of convection, drift and diffusion and gets deposited on the condensing wall or leave the domain through outlet. The effect of gravity and inertia on deposition is negligible as the test section is vertical and the flow acceleration infinitesimal. Therefore, the fog droplet deposition is largely induced by turbulent and Brownian diffusion with equal contributions from both. The droplet deposition gradually increases from zero at the inlet to a maximum towards the end of the channel as observed from the fog density distribution (Fig. 6). Some droplets also diffuse away from the walls where they get evaporated and adds to the steam content. However, the diffusive transport of fog droplets is very low when compared with the convective transport by the flow and hence, the change of droplet diameter from $1\mu m$ to $100\mu m$ had only marginal effects ($< 0.1\%$) on the results. Therefore, the results discussed here are from simulation where droplet diameter is $1\mu m$. The maximum fog volume fraction was $<< 1\%$ which is within the modelling assumptions. The total wall heat flux, wall temperature and near-wall temperature from simulation are compared with the experimental data in Fig. 7 and 8. The total wall heat flux is an indirect measurement of condensation rate because condensation wall heat flux contributes to 90% of wall heat flux compared to sensible wall heat flux (Kumar et al., 2021). The bulk condensa-

tion model coupled with wall condensation reduced the total wall heat flux and wall temperature by 2 % making it closer to the experiment thus improving the prediction accuracy. The latent heat release as a result of bulk condensation increased the near wall temperature for $y < 30mm$ (Fig. 8) augmenting wall heat flux but, the decrease in wall condensation heat flux by a higher amount resulted in the net reduction of total wall heat flux. Also, the vaporization of droplets diffusing away from the wall cooled the surrounding gas mixture by absorbing latent heat for vaporization indicated by slightly lower temperature at $y > 30mm$. The condensation near the wall and evaporation away from the wall is demonstrated using the mass transfer rate profile in Fig. 8. The mass transfer rate is zero on wall because bulk condensation(or evaporation) is zero in the near wall cell as wall condensation is responsible for mass removal in this cell as explained before. The bulk condensation reduced the integral wall condensation rate by around 10 %, however, the net condensation rate (wall + bulk) remained same. The change in the results by the inclusion of bulk condensation is small (2 %) primarily due to the same net condensation rate and secondarily because of limitation of condensation (wall and bulk) only to regions near the wall owing to the conditions inside the channel.

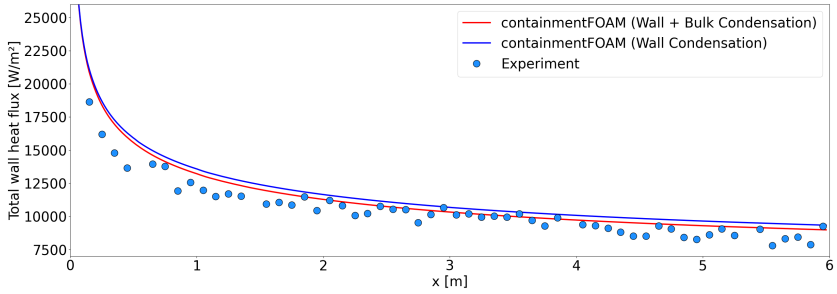

Figure 7: Comparison of total wall heat flux distribution along the cooled wall in SETCOM2D with and without bulk condensation

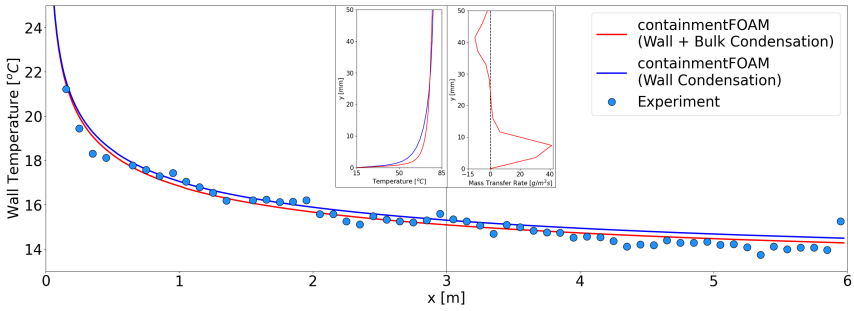

Figure 8: Comparison of wall temperature along the cooled wall in SETCOM2D with and without bulk condensation. Inset: Temperature and mass transfer rate profile near the condensing wall at x = 3 m

3.4. ThAI TH2 experiment validation

The TH2 experiment (T. Kanzleiter, 2002) at ThAI facility (ThAI=Thermal hydraulics, Hydrogen, Aerosols, Iodine) operated by Becker Technologies GmbH investigates the formation and breakup of atmospheric stratification in the vessel by injecting hot steam into a wet air mixture. Phase 1 of the experiment is simulated where test vessel is heated by continuously feeding saturated steam through a toroidal feed pipe inlet at the upper portion. The objective of this validation case is to assess the capabilities of the bulk condensation model in estimating the transient pressure and temperature inside the vessel. The computational domain is simplified by considering an axisymmetric simulation with mesh and inlets as shown in Fig. 9. The 2D axis-symmetric mesh used for the simulations here is a fine mesh with $y^+ \approx 1$ which is developed based on previous ThAI vessel simulations by Kelm et al. (2016) and Kumar et al. (2020), hence, mesh independency study is not explicitly performed. Also, since the passive scalar fog transport model cannot handle large deposition of fog on walls, a deposition boundary condition is used to remove fog reaching the walls. The vessel is initially filled with an air-steam mixture of 99 % relative humidity at 24 ^oC and 1.042 bar pressure and steam is injected at a mass flow rate of 35 g/s. For examining the effect of fog droplet diameter also on the results, the simulation was run at two different droplet diameters of 1 μm and 25 μm which were selected based on previous simulations by (Zhang and Laurien, 2014) and measurements from other ThAI experiments.

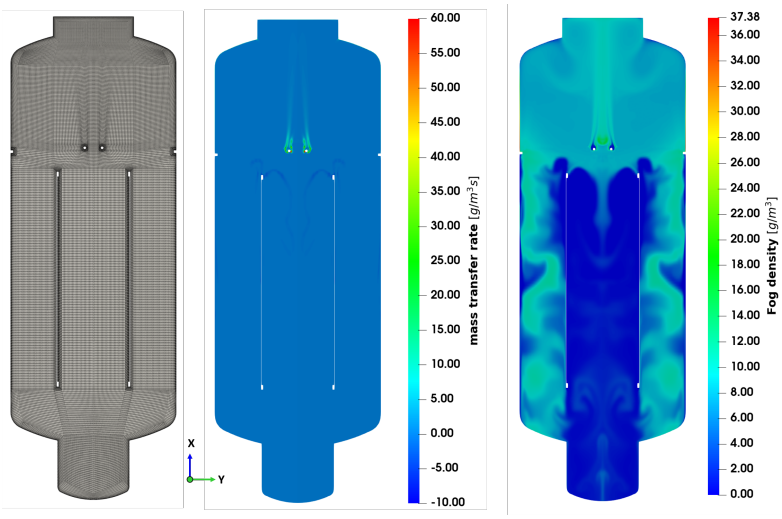

Figure 9: Left:Computational mesh for axisymmetric simulation of ThAI TH2 experiment. Middle: Fog formation (and evaporation) rates distribution inside the vessel at time = 1500 s. Right: Fog distribution inside the vessel at time = 1500 s

The fog formation rate and its distribution within the vessel at time = 1500 s is shown in Fig. 9. The condensation primarily occurs near the steam injection

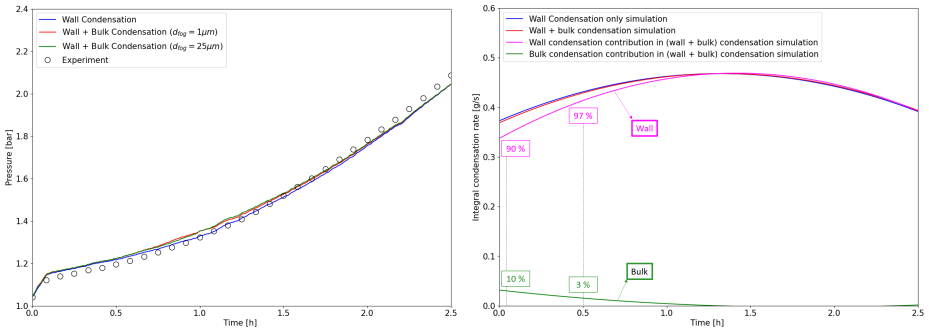

(a) (b)

Figure 10: (a):Transient pressure variation in the TH2 vessel wrt different condensation modes and droplet diameters. (b): Comparison between integral condensation rates with and without bulk condensation and contribution from each mode in case of combined condensation($d_{fog} = 1\mu m$)

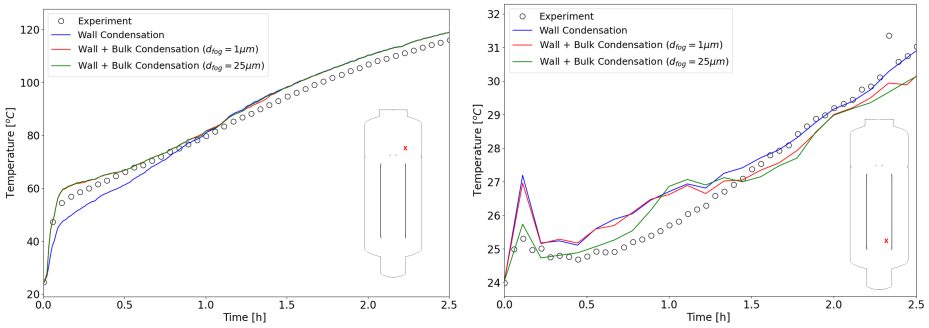

(a) (b)

Figure 11: Transient temperature variation in the upper(a) and lower(b) regions of the vessel wrt different condensation modes and droplet diameters

region and upper portion of the vessel to where injected steam traverses due to its lower density compared to the surrounding gas mixture. The fog droplets get transported to the upper region by the convection currents and then slowly drift towards the sump region predominantly due to gravity effect. The turbulent and Brownian diffusion aid the mixing of the fog droplets with the gas mixture. Fig. 10a showing the pressure and temperature variation inside the vessel with time indicates close agreement of the simulation with the experiment. The bulk condensation and droplet diameter does not have notable effect on the vessel pressure. This is because, the vessel pressure is influenced primarily by the net condensation rate and secondarily by the contribution of bulk condensation rate to the net rate. If bulk condensation contribution is high, then the accompanying latent heat release and following temperature rise will be high, resulting in a higher increase the vessel pressure. From Fig. 10b, we can observe that the net condensation rate change is marginal with the inclusion of bulk condensation.

Also, the bulk condensation rate contribution to the net rate is only 10 % at the beginning and becomes 3% in half hour and gradually diminishes to zero in one and half hours. The change in integral condensation rate with droplet diameter is negligible and hence the rates with droplet diameter = $1\mu m$ only is shown in Fig. 10b. During the initial time period ($t < 0.5h$), the steam and condensation regions are very narrow and therefore, the change in vessel pressure with bulk condensation inclusion is small. As time progresses, steam spreads to more regions and so does condensation. The is why the pressure with bulk condensation is slightly higher than that with only wall condensation after $t = 0.5h$ owing to the latent heat release to the gas mixture during condensation. This is also indicated by the higher temperature with bulk condensation in the upper region of the vessel (Fig. 11a). The addition of bulk condensation improved the temperature prediction accuracy by 5% in upper region during the initial stages of steam injection while the droplet diameter had no effect. The condensed fog droplets in the upper region get transported to the lower region by gravity and other effects where they get evaporated by absorbing the latent heat from the gas mixture, thereby cooling the surrounding mixture. This results in a reduced temperature in the lower regions as observed in Fig.11b. The droplet diameter affects the temperature distribution mainly in the lower region because the larger droplets ($d_{fog} = 25\mu m$) can easily drift towards the sump while smaller droplets ($d_{fog} = 1\mu m$) tends to follow the gas flow path. The larger droplet diameter is able to predict the temperature at lower region with 6% better accuracy than the smaller droplet during the initial stages of the simulation. The vessel atmosphere becomes saturated, and integral bulk condensation becomes negligible after 1.5 hour as indicated by the overlap of the pressure plots with and without bulk condensation. In the saturated atmosphere, the suspended droplets get transported to different regions depending on their diameter where they may evaporate and then re-condense at some other region indicated by the differences in temperature. Hence, modelling of fog droplet diameter considering nucleation, coalescence and breakup phenomena is important in predicting the vessel conditions more accurately. As the fog reaching the walls were removed from the computational domain, the maximum fog volume fraction in this simulation was $<< 1\%$ which is well within the modelling assumptions. The key inference from the ThAI TH2 validation study is that bulk condensation(or evaporation) and droplet diameter will have a substantial effect on the local temperature of the gas mixture which is an important parameter for reactor safety especially in the presence of hydrogen.

4. Conclusions

In the present work, the development of bulk condensation model and the transport of fog droplets as a passive scalar and its re-evaporation is discussed in detail. The bulk condensation (and evaporation) is modelled by maintaining the mixture at saturation temperature locally at all times. The fog transport is made computationally simple and efficient by considering fog as passive scalar in an Eulerian framework interacting with the primary flow only through source

and sink terms. The deviation (or drift) of fog droplets from the primary flow field was also modelled by considering the effect of inertia, gravity, drag and diffusion forces. The model was implemented in *containmentFOAM* solver based on OpenFOAM focusing on simulating containment thermal hydraulics. The fog transport formulation is based on the assumption that fog volume fraction is low ($< 1\%$) so that the droplet-droplet interactions and its effect of the gas flow field can be neglected. The present model also assumes that the droplet diameter is fixed and evolution by nucleation, coalescence and breakup are neglected. However, the effect of droplet diameters were investigated for the validation cases to understand its consequence on the results. The diameters for ThAI and bent pipe validation cases were chosen from previous simulations and experimental studies, and had notable effect on the local temperature inside the ThAI TH2 vessel and deposition efficiency in the bent pipe. For the Mollier case, the diameter effect was insignificant because drift effects were not considered and for SETCOM case, the dominance of convective flow over other forces caused only marginal deviations in results due to droplet diameter variation. The droplet diameters for simulations should be selected based on the extremum values measured from the corresponding experiments or from experiments with similar conditions.

The condensation (and evaporation) model validation with Mollier diagram accurately predicted the amount of fog formed and the final mixture temperature after condensation(and evaporation). The droplet drift from the gas flow path due to external forces was modelled using Stokes and Manninen approaches. The comparison with droplet deposition on bent pipes found in open literatures revealed that the Stokes model is superior in estimating the drift velocity at all range of Stokes numbers than the Manninen model. The consideration of fog formation near the cooled wall in addition to wall condensation in SETCOM experiment improved the total wall heat flux and wall temperature prediction by containmentFOAM and also provided new insights into the boundary layer temperature profiles. Further validation studies on ThAI TH2 experiment indicated that the vessel temperatures are better predicted at some locations by including bulk condensation effects and droplet diameter is a significant parameter affecting the local temperatures. Ongoing and future work aims at developing and implementing droplet size prediction models in an Eulerian framework using Population Balance Model(PBM) by including the effects of nucleation, coalescence, growth by condensation and shrinkage by evaporation for droplets. Furthermore, the accumulation of condensate is investigated by transferring the passive scalar transport into a VOF approach.

Acknowledgements

The authors gratefully acknowledge the German Ministry for Economic Affairs and Energy for funding the national THAI-1 project (No. 150 1218) and Becker Technologies (Eschborn, Germany) for carefully documenting and sharing the THAI experimental data. Furthermore, we thank the German Acedemic

Exchange Service (DAAD) for funding the PhD position under the 'DAAD-Research grants for Doctoral Program'.

References

Babić, M., Kljenak, I., Mavko, B., 2009. Simulations of tosqan containment spray tests with combined eulerian cfd and droplet-tracking modelling. Nuclear Engineering and Design 239, 708 —- 721.

Cheng, Y.S., Wang, C.S., 1981. Motion of particles in bends of circular pipes. Atmospheric Environment 15, 301 – 306.

Ding, P., Liu, Y., Wang, B., Li, W., Wang, J., 2017. The homogeneous and lagrangian tracking approaches of the spray simulation in the containment. Annals of Nuclear Energy 101, 203 —- 214.

Frederix, E.M.A., Kuczajd, A.K., Nordlundd, M., Veldmanc, A.E.P., Geurts, B.J., 2017. Eulerian modeling of inertial and diffusional aerosol deposition in bentpipes. Computers and Fluids 159, 217 – 231.

Hinds, W.C., 1999. Aerosol Technology. John Wiley & Sons, 2^{nd} edition.

Kelm, S., Kampili, M., Kumar, G.V., Sakamoto, K., Liu, X., Kuhr, A., Druska, C., Prakash, K.A., H.-J. Allelein, booktitle=18th International Topical Meeting on Nuclear Reactor Thermal Hydraulics (NURETH-18), y.a..P.O.U., . Development and first validation of the tailored cfd solver 'containmentfoam' for analysis of containment atmosphere mixing.

Kelm, S., Kampili, M., Liu, X., George, A., Schumacher, D., Druska, C., Struth, S., Kuhr, A., Ramacher, L., Allelein, H.J., Prakash, K.A., Kumar, G.V., Cammiade, L.M.F., Ji, R., 2021. The tailored cfd package containmentfoam for analysis of containment atmosphere mixing, h2/co mitigation and aerosol transport. Fluids 6, 100.

Kelm, S., Lehmkuhl, J., Jahn, W., Allelein, H.J., 2016. A comparative assessment of different experiments on buoyancy driven mixing processes by means of cfd. Annals of Nuclear Energy 93, 50 – 57.

Kelm, S., Muller, H., Hundhausen, A., Druska, C., Kuhr, A., Allelein, H.J., 2019. Development of a multi-dimensional wall-function approach for wall condensation. Nuclear Engineering and Design 353.

Kumar, G.V., Cammiade, L.M.F., Kelm, S., Prakash, K.A., Rohlfs, W., 2021. Implementation of a cfd model for wall condensation in the presence of non-condensable gas mixtures. Applied Thermal Engineering 187, 116546.

Kumar, G.V., Kampili, M., Kelm, S., Prakash, K.A., Allelein, H.J., 2020. Cfd modelling of buoyancy driven flows in enclosures with relevance to nuclear reactor safety. Nuclear Engineering and Design 365, 110682.

Manninen, M., Taivassalo, V., , Kallio, S., 1996. On the mixture model for multiphase. VTT Publications 288, Technical Research Center of Finland.

Menter, F., Esch, T., 2001. Elements of industrial heat transfer predictions, in: Proceedings of the 16th Brazilian Congress of Mechanical Engineering (COBEM-2001).

Mollier, R., 1929. Ein neues diagramm für dampf-luft gemische. Z. VDI 73, 1009 – 1013.

Pilou, M., Tsangaris, S., Neofytou, P., Housiadas, C., Drossinos, Y., 2011. Aerosol science and technology inertial particle deposition in a 90° laminar flow bend: An eulerian fluid particle approach. Aerosol Science and Technology 45, 1376 – 1387.

Pui, D.Y.H., Romay-Novas, F., Liu, B.Y.H., 1987. Experimental study of particle deposition in bends of circular cross section. Aerosol Science and Technology 7, 301 – 315.

Siemens, 2007. Psychrometric Chart - Structure and Application. Siemens Switzerland Ltd.

T. Kanzleiter, 2002. Experimental facility and program for the investigation of open questions on fission product behaviour in the containment (ThAI = Thermal Hydraulics, Aerosols, Iodine). Technical Report. ThAI-Experiment TH2, Test Report to Reactor Safety Research Project No. 150 1218.

Vyskocil, L., Schmid, J., Macek, J., 2014. Cfd simulation of air–steam flow with condensation. Nuclear Engineering and Design 279, 147 – 157.

Wilke, C., 1950. A viscosity equation for gas mixtures. The Journal of Chemical Physics 18.

Zhang, J., Laurien, E., 2014. 3d numerical simulation of flow with volume condensation in presence of non-condensable gases inside a pwr containment, in: W. E. Nagel, D. H. Kröner, M. M. Resch (eds.)High Performance Computing in Science and Engineering '14: Transactions of the high performance computing center, stuttgart (HLRS) 2014, Springer. pp. 479 – 497.